REPORT DOCUMENTATION PAGE

Form Approved
OMB No. 0704-0188

1. REPORT DATE *(DD-MM-YYYY)*	2. REPORT TYPE	3. DATES COVERED *(From - To)*
08/29/2019	Final	03-01-2016 to 05-31-2019

4. TITLE AND SUBTITLE
Integration of Biomolecular Recognition Elements with Solid-State Nano-Devices for Chemical Sensors with Specificity

5a. CONTRACT NUMBER

5b. GRANT NUMBER
N00014-16-1-2279

5c. PROGRAM ELEMENT NUMBER

6. AUTHOR(S)
Willis, Brian G.

5d. PROJECT NUMBER

5e. TASK NUMBER

5f. WORK UNIT NUMBER

7. PERFORMING ORGANIZATION NAME(S) AND ADDRESS(ES)
University of Connecticut
Office of Sponsored Programs
438 Whitney Rd. unit 1133
Storrs, CT 06269

8. PERFORMING ORGANIZATION REPORT NUMBER

9. SPONSORING/MONITORING AGENCY NAME(S) AND ADDRESS(ES)
same

10. SPONSOR/MONITOR'S ACRONYM(S)
UCONN

11. SPONSOR/MONITOR'S REPORT NUMBER(S)

12. DISTRIBUTION/AVAILABILITY STATEMENT
Approved for Public Release; distribution is unlimited

13. SUPPLEMENTARY NOTES
Program Manager: Joong Kim, Joong.kim@navy.mil, EXP WARFARE & COMBATING TERRORISM DEPT
875 N. Randolph St, Arlington VA 22203-1995

14. ABSTRACT
We investigated nanomaterials and nanodevices for chemical sensors with applications in explosives detection. The work addresses limitations of existing chemical sensors for not only detecting, but also identifying chemical signatures in open air environments. The work is organized around a "large N" hypothesis, which proposes that robust chemical detection in open environments can be achieved using large arrays of nanoscale elements integrated into sensor chips made using microfabrication technology. Arrays of 64 individually addressable sensing elements were analyzed by machine learning using methods that are scalable to sensor chips with hundreds, thousands, or even more independent elements.

15. SUBJECT TERMS
Explosives Detection Chemical Sensors Nanofabrication Nanomaterials VOCs UNIFAC Machine Learning

16. SECURITY CLASSIFICATION OF:			17. LIMITATION OF ABSTRACT	18. NUMBER OF PAGES	19a. NAME OF RESPONSIBLE PERSON
a. REPORT	b. ABSTRACT	c. THIS PAGE		30	Brian G. Willis
					19b. TELEPHONE NUMBER *(Include area code)* 860 486 9429

Final Report

Integration of Biomolecular Recognition Elements with Solid-State Nano-Devices for Chemical Sensors with Specificity

University of Connecticut

Award # N00014-16-1-2279

Technical Contact

Brian Willis
Chemical Engineering
191 Auditorium Rd. Unit 3222
Storrs, CT 06269
brian.willis@uconn.edu
860-486-9429

Period of Performance

March 1, 2016 – February 28, 2019

Abstract

We investigated nanomaterials and nanodevices for chemical sensors with applications in explosives detection. The work was designed to address several deficiencies of existing sensors related to speed, reversibility, sensitivity, size, power, and cost. In particular, this work addresses limitations of existing chemical sensors for not only detecting, but also identifying chemical signatures in open air environments. The work is organized around a "large N" hypothesis, which proposes that robust chemical detection in open environments can be achieved using large arrays of nanoscale elements integrated into sensor chips made using microfabrication technology. The current work achieved arrays of 64 individually addressable sensing elements, and the methods are scalable to sensor chips with hundreds, thousands, or even more independent elements. Scalability is especially exciting because results are already very good for the small arrays reported here. Using machine learning methods, including discriminant analysis, k-nearest neighbors, and random forest, sensor chips achieve classification accuracies consistently in the range of 95-100% for test sets of 20 volatile organic compounds (VOCs) and 39 commercial Teas.

The VOC test set was designed to gain deeper understanding into how our sensors work at the molecular scale, and the Tea set was designed to test performance for complex odors. The sizes of the two test sets and the good performance of the classification algorithms are state-of-the-art for chemical sensors. In the future, machine learning will benefit from larger datasets using sensor arrays with more devices. We observe that our sensors function like artificial noses, similar to canines trained to detect explosives. The devices are not inherently tuned to detect particular chemicals, but can be trained to distinguish many types of odorant signatures. Once a sensor chip is trained, it can identify unknown odorants through machine learning classification algorithms. Besides VOCs and Teas, we also demonstrate sensing for materials related to explosives, including ammonium nitrate (AN) and trinitrotoluene (TNT). The sensors are fast and reversible with characteristic "ON times" of 100 ms or better. Further research should enable high speed sensors that can reliably detect and classify many types of explosives and chemical precursors.

The performance of our sensors has exceeded expectations and raises questions about how they function so well. Two different modeling approaches were initiated during this work to better understand how sensor devices interact with odorants at the molecular and device scales. The first approach uses UNIFAC to model chemical interactions between sensing materials and VOC analytes. Initial results show trends that qualitatively match experiments and indicate that rational design of sensor materials may be possible from basic chemical principles. The second model seeks to understand sensor device properties based on configurational effects of nanoparticle networks. While molecular scale chemical interactions were expected, configurational effects are less intuitive. Initial results suggest sensor performance is boosted by variations of particle configurations in particle networks. The configurational heterogeneity generates new information for sensor elements and promotes classification accuracy.

1. Introduction & Methods

Nanomaterials and nanodevices are especially promising for chemical detection because they are intrinsically fast and sensitive, and their simplicity allows for organization into complex hierarchical devices. This work has investigated chemiresistors as transducers using nanoparticle sensing elements. Chemiresistors are among the simplest devices for chemical sensing with robust detection via electrical resistance measurements using two terminal devices. Very simply, chemiresistors are circuit elements that change resistance when exposed to different chemical environments. The sensors have no inherent specificity to any particular agents and respond broadly to different chemical environments. The method of sampling is through exposure to, or collection of vapors emanating from a source.

In this work, the term 'nanoparticles' refers to core-shell nanostructures with metallic cores and organic shell layers. Metallic cores are most often gold (Au), but other metals like palladium (Pd) have also been used. (Note, the amount of material used is so miniscule that precious metal cost is not significant). Core sizes range from a few nm to 100 nm diameter, with most of our work using 10 – 20 nm diameter particles. The organic shell layers are composed of small molecules covalently bonded to metallic cores most often through thiol or amine chemical linkages. The chemical structures of the organic shell layers, including molecular organization, stacking, and packing density are generally unknown, and may vary significantly with different types of organic molecules. In this work, we refer to our core-shell particles as *monolayer capped nanoparticles*. It is assumed that the organic shells are limited to single (mono) layer thickness, but it is likely that residual solvents and unattached amines and thiols may also be present. The synthesis of monolayer capped nanoparticles is an advanced area of chemistry and is not discussed here. Many types of

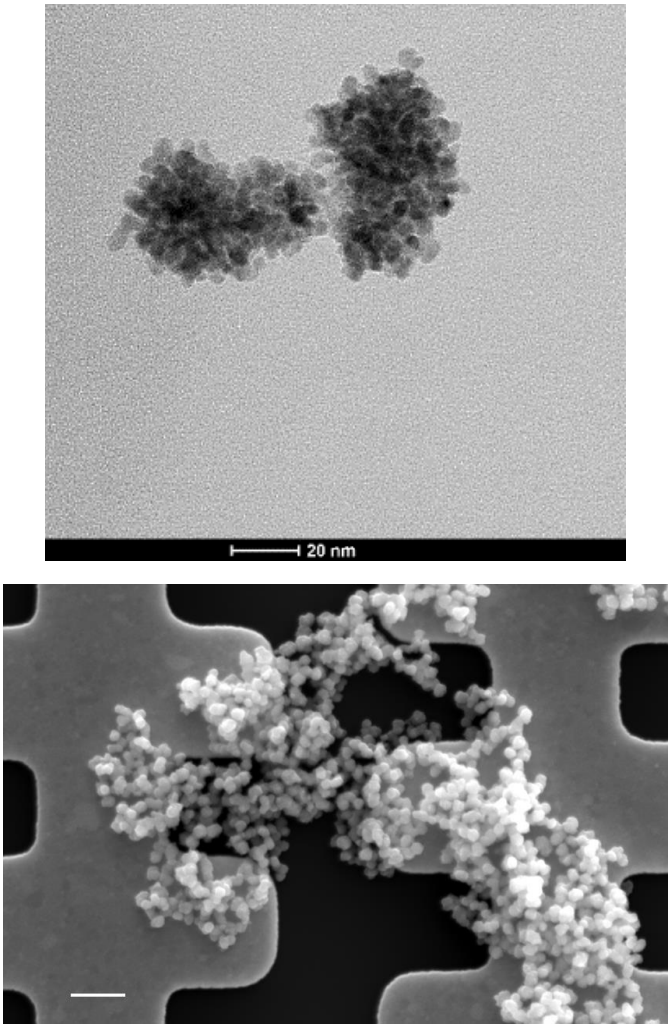

Figure 1. upper: TEM of OLA-PdNP (scale bar = 20 nm); lower: SEM of OLA-PdNP between electrodes (scale bar = 1 μm).

Table 1. Nanoparticle types and abbreviations used in this work

DDA	dodecylamine
TDA	tetradecylamine
HDA	hexadecylamine
ODA	octadecylamine
OLA	oleylamine
-	citrate
DMAP	4-(dimethylamino)pyridine
CTAB	cetrimonium bromide
CTAC	cetrimonium chloride
MPA	3-mercaptopropionic acid
HBA	4-hydroxybenzoic acid
ATP	4-aminothiophenol
MUA	11-mercaptoundecanoic acid
PEG-thiol	methoxy polyethylene glycol thiol
-	dodecanethiol

particles can be purchased commercially from standard vendors like Sigma-Aldrich. Figure 1(a) shows a transmission electron microscope (TEM) image of aggregates of nanoparticles, and Figure 1(b) shows a scanning electron microscope (SEM) image of particles arranged on a substrate between micro-fabricated electrodes. The organic shell layers are present, but not resolved in these electron microscopy images. It can be seen that the particles form aggregates with random configurations of varying connectivity.

Key advantages of nanoparticles as sensing materials are their inherent small size, ease of synthesis, and limitless chemistry. The small size makes it possible to integrate nanoparticles into nanoscale devices and form large arrays of tiny devices. Moreover, nanosize makes them inherently fast since molecular transport processes are rapid at the nanoscale. Molecular diffusion is very fast through small clusters of particles that contain only a few layers. The possible composition of the organic shells is very diverse with all of the available tools of organic synthesis, and can also be extended to biomolecules such as DNA aptamers. Biomolecules can bring new types of detection motifs including molecular recognition through shape dependent host-guest interactions. Thus, nanoparticles offer a rich library of chemical properties that can be exploited for chemical sensors, including biomolecular recognition elements. The only practical limitation is that the aggregates of nanoparticles must have sufficient conductivity to form electrically resistive circuit elements. Molecules that are too large or insulating may form device elements with resistance too high to measure. Thus, most molecular capping agents currently used are about 1 – 2 nm in size. Table 1 shows a collection of capping agents that have been studied in this work. Molecular capping agents are chosen based on their availability, chemical diversity, and sensor performance. A large collection of materials is desirable, and in the future we envision devices with tens to hundreds of different organic shell layers.

We define sensor elements as individually addressable electrode pairs loaded with nanoparticles, like Figure 1(b). We have investigated both microscale and nanoscale electrodes for making devices, where electrodes are fabricated on substrates such as glass or silicon. Sensor elements are enabled by collecting and trapping nanoparticles in the regions between pairs of electrodes to form resistive circuit elements. Two methods have been explored for adding/ loading nanoparticles into electrode arrays. The first is simple drop casting with a micropipette. A 1 microliter droplet of particle solution is applied over the electrodes. Particles remain on the substrate after the solvent dries. The advantage of this approach is simplicity; it provides a high yield of working devices. The disadvantage is little control over the placement of nanoparticles, and each

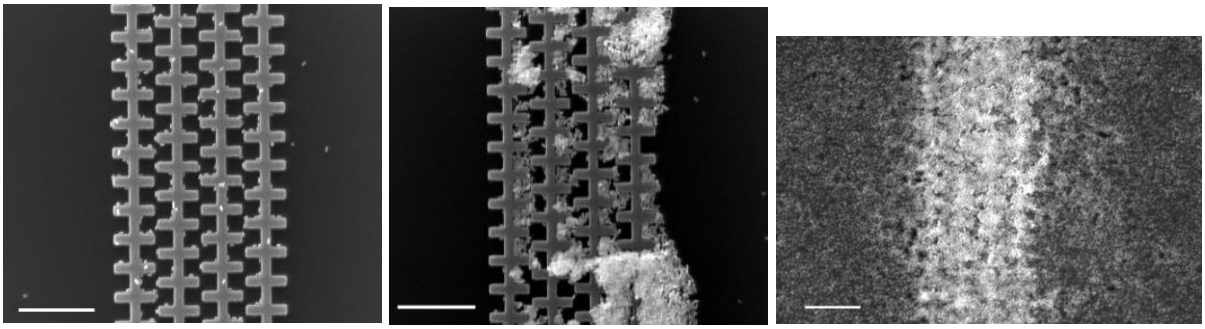

Figure 2. SEM images of nanoparticle assemblies under DEP. Left: 1 MHz, 4 V, 1 min; Center: 1 MHz, 4 V, 2 min; Right: 1 MHz, 4 V, 4 min. Scale bars for all three images are 1 μm. The resistances corresponding to each device are 10, 7, and 7 kΩ, respectively.

nanoparticle aggregate is different. The area coverage is also not typically uniform so that not all areas of the electrodes are used. The other problem is that, although tiny, the microliter droplet spreads out several mm on a sensor chip, which limits our ability to create multi-particle sensor chips. Figure 1(b) is an example of a microscale device made using drop casting.

The drop casting technique does not extend from micro to nanodevices because the nanoelectrodes occupy substrate areas so tiny that it becomes unlikely that randomly deposited nanoparticles will cover and span nanoelectrodes. For nanoscale devices, we use dielectrophoresis (DEP) to attract particles from solution into the high field regions of the nanoelectrodes. Figure 2 illustrates an example of nanoscale sensor elements made using DEP. The number of particles increases with time from left to right. Compared to drop casting, DEP provides better control over the placement and numbers of nanoparticles in each device junction. However, the method requires the application of high frequency (1 MHz) AC voltages to the electrodes while immersed in nanoparticle liquid solution. Nanoparticles are attracted to high electric field regions near sharp corners and constrictions between electrodes. The castellated electrode shape in Figure 2 is designed to optimize the high field regions for a greater collection force. The DEP method works well for nanoscale devices, but requires electrical connectivity to each device.

Most of our classification experiments used sensor chips with large electrode arrays made by drop casting with micron size electrodes. DEP is not possible with micron sized devices because exceedingly high voltages would be needed to achieve the necessary electric fields. For nanoscale devices the applied voltages are only a few (1 - 4) volts AC, but impractical voltages >> 10 VAC would be required for micron scale devices. DEP was used with nanoscale devices on smaller sensor chips mounted on TO packages for various experiments, but not for the classification studies. The primary advantage of nanoscale devices is speed and layout density, but the microscale devices are easier to process and more than adequate for most of our work. In future work, more effort can be dedicated to making sensor chips with large arrays of nanoscale elements using DEP, but it was not necessary to reach our current goals.

Sensor elements are arranged into arrays to make integrated sensor chips. The sensor chips are fabricated on 100 mm silicon wafers and each chip is near 1 x 1 cm^2 size. During sensing experiments, the resistances of every sensor element are measured separately and simultaneously as a function of time. Raw data are resistance vs. time measurements for each sensor element. These raw data are processed with peak recognition algorithms to produce $\Delta R/R_o$, which is the most useful form of the data. The processed data normalizes for the different baseline resistances of each sensor element, R_o.

The mechanism for chemiresistor sensing with nanoparticles is generally known to follow equation (1)

$$\frac{\Delta R}{R} = e^{\beta \Delta \delta} \cdot e^{\frac{\Delta E_a}{kT}} - 1 \qquad (1)$$

where β is a tunneling decay constant specific to the molecular capping agents, δ is the edge-to-edge distance between nanoparticle cores, E_a is an activation energy related to Coulomb blockade energy, k is the Boltzmann constant, and T is temperature in Kelvin. The sensor response is represented by $\frac{\Delta R}{R}$, which is the experimental change in resistance divided by the baseline resistance, R_o. R_o is the resistance measured when there are no analytes present. The equation is derived for an electronic charge transport mechanism based on electron tunneling between particles. The first term shows that the tunneling rate is exponentially dependent on the distances between particles, with additional effects of particle size and medium permittivity through E_a. Equation (1) predicts sensing action through modulation of particle - particle distances ($\Delta\delta$) and the permittivity (ε) of the organic medium. In the present studies, permittivity effects are less important because our particles are relatively large. Our emphasis is on swelling effects ($\Delta\delta$).

When chemiresistors are exposed to odorants, volatile molecules partition into the organic shell layers according to basic thermodynamic principles (see later discussion of UNIFAC modeling). The solvation of volatile odorants into the condensed organic phases causes swelling and increases in particle - particle distances, which causes a positive $\Delta\delta$. Swelling can be simply understood as a consequence of volume expansion from insertion of odorants into the sensor materials, like a dry sponge absorbing water. (In some less common cases, vapors can induce apparent negative $\Delta\delta$, but we do not generally observe those effects in our studies). The dielectric properties of the odorants can also modulate the medium permittivity, but for non-polar molecules the main effect is swelling. Note that we use the terms 'odorant', 'analyte', 'vapor', 'chemical,' and 'target' interchangeably.

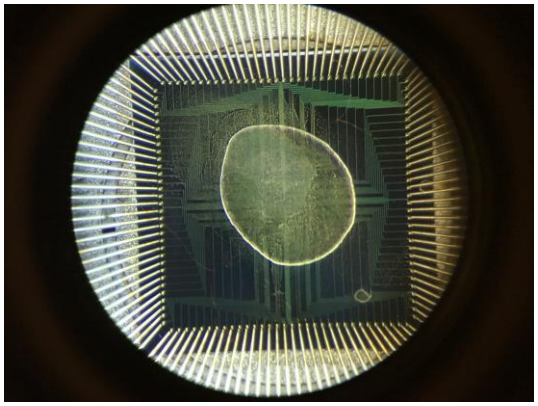

Figure 3. Optical image of a sensor chip under test through a microscope objective.

In our experiments, resistances are measured using a multimeter instrument combined with a multiplexer to record many devices simultaneously. Our experimental arrangement uses a probe card to electrically connect 64 two-terminal devices for rapid scanning of all devices. Figure 3 shows an optical image of a 128 pin probe card connected to a device under test. A dried droplet of nanoparticle solution is evident in the center of the chip.

Experiments involve measuring resistances vs. time while alternately pulsing and purging ('sniffing') chemical vapors. Our chemical sampling configuration uses a syringe pump for delivering vapors through a stainless steel tube to a sensor chip mounted in a probe station (Figure 5). For experiments using VOCs, vapors are generated by adding a small (microliter) droplet of source material to a syringe tube and allowing it to come to equilibrium in air. For commercial Tea samples and solids like ammonium nitrate, a few µg to mg of solids are added to syringe tubes. (We sense dry Tea leaves, not the brewed liquid). During sampling, vapors are diluted with a second stream of gas in a mixer located upstream of the sensor chip under test. The dilution serves multiple purposes: (1) it purges away vapors after each sampling pulse ('sniff'), (2) it provides control over analyte concentration by dilution, and (3) it limits the vapor concentration to avoid possible damage of sensors at high concentrations.

Other sampling methods also work, but we have found that a syringe pump provides good control over the volume of vapor / air mixture sampled and the rate of injection and length of pulses. These sampling parameters also allow control of the vapor analyte concentrations. Typical pulse lengths are a few seconds or shorter, usually long enough to achieve a steady response with a square wave shape. Other sampling arrangements that we have used include squeeze bottles placed near a sensor chip in open air, or simply wafting vapors over a sensor chip. In addition, smaller chips have been mounted on TO packages and moved to and fro a source. Each of these methods works, but they do not provide the same level of control as the syringe pump arrangement. Moreover, the probe station is not mobile, so movements that are possible with a TO package are not practical with a probe station.

Figure 4 shows an example of raw data for a sensing experiments using 2,4-DNT (dinitrotoluene) as a target. The figure shows a subset of 16 out of 64 sensors, each recording resistance vs. time traces for a series of vapor pulses. The multiplexing rate is sufficiently high so that all sensors are sampled in less than 1 second for near simultaneous responses. The raw data for all devices are processed using automated peak recognition and baseline subtraction routines to quantify each sensor device response as a change of resistance. The data are converted into $\Delta R/R_o$ values where ΔR is the resistance change and R_o is the initial baseline resistance. The later varies from device to device because each device has different numbers and arrangements of particles. For typical vapor concentrations near 1 - 10% of the saturation pressure (p/p_{sat}), the magnitude of $\Delta R/R_o$ responses is near 1 – 10%, but varies significantly for different analytes and sensor materials. It is precisely these variations and their patterns that provide the ability to recognize and classify odorants.

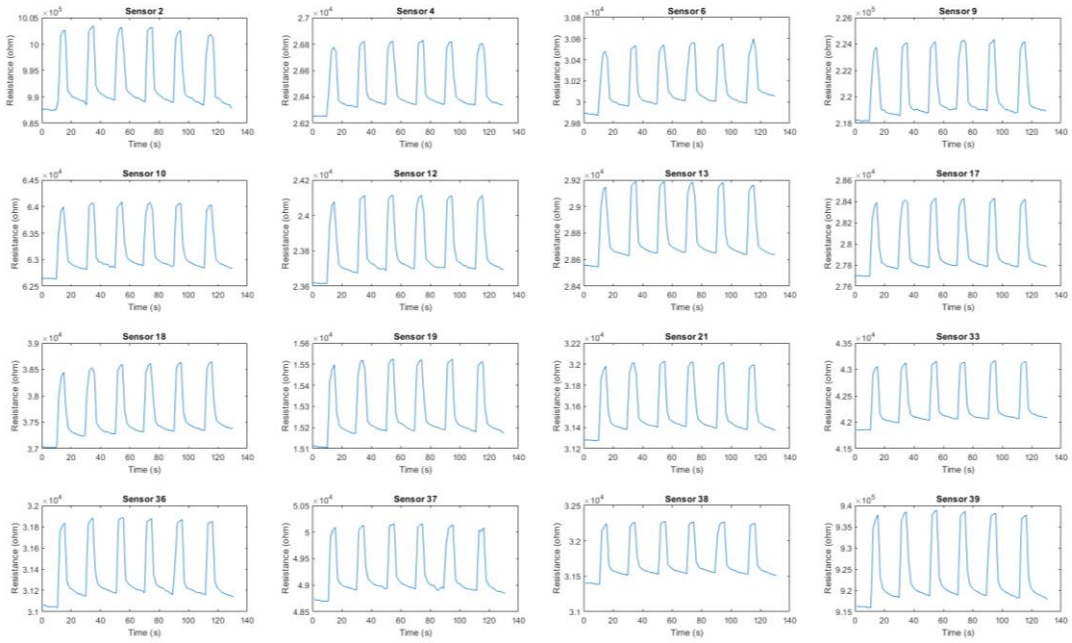

Figure 4. Raw data for a subset of 16 sensors out of 64 that simultaneously detect 2,4-DNT vapor using DMAP as the sensing material.

Experimental $\Delta R/R_o$ data are collected from each device for each odorant/ air pulse and assembled into a data matrix. The data matrix contains n by m rows and columns where each row represents a vapor pulse and each column is a sensor device response. For example, with 48 working sensors, 20 chemicals in a test set, and 8 samples per chemical, we would have a 160 x 48 data matrix. The data matrix format is standard for multivariate analysis and machine learning (ML) algorithms. We have used the Matlab Classification App to analyze results with a number of different approaches (https://www.mathworks.com/ products/ matlab.html). The most useful and accurate have been linear discriminant analysis (LDA), k-Nearest Neighbors (KNN), bagged trees (BT), and Random Forests (RF). These methods are considered 'supervised' because they use a-priori knowledge of the targets to train the algorithms, similar to training canines to recognize explosives. Once a sensor is trained, it can predict the 'classes' of unknown samples. In the context of chemical sensing, the classes are the identity of different odorants. Standard analysis involves cross-validation to assess classification accuracy. Cross validation divides each data set into subsets of training and test samples. The training set is used to train the algorithm and the accuracy is evaluated by testing the ability to predict the test set. The cross validation approach is equivalent to taking additional samples and not including them in the training set, and then testing the algorithm accuracy with the additional samples.

We have also used principal components analysis (PCA) to analyze our data. PCA is called an 'unsupervised' method because it analyzes datasets without any prior knowledge of the groupings of different samples. PCA does not directly identify unknown

odorants, but the analysis provides some visual indication of the natural groupings of the samples. Targets with similar chemical properties will naturally group together and the groupings can be used to qualitatively rationalize sensor properties.

Our data sets are relatively small compared to what is possible, yet we achieve accuracies consistently above 90% using large test sets of 20 VOC chemicals and 39 Teas. The ML algorithms have the capability to scale-up to much larger datasets and we expect that sensor chips with hundreds or thousands of sensors and automated sampling could be rapidly trained to detect and classify target sets with hundreds of different analytes. Alternatively, smaller test sets could be identified with very high accuracy.

In addition to classification, the ML methods have the ability to provide confidence intervals on chemical detection results. The algorithms can also be adjusted to consider the relative costs of false positives and false negatives. These are features we have not yet included in our analysis.

2. Experiments

We demonstrate the performance of our sensor arrays using two large datasets. One is a collection of 20 different VOCs, and the other has 39 commercial Teas. The purpose of the VOC set is to provide data that can be used with our modeling studies to better understand how our devices work, see later discussion of the UNIFAC method. The purpose of the Tea set is to demonstrate how sensors perform with solid materials and complex, multicomponent odorants. We also studied nitrates and other materials more relevant to explosives detection using smaller test sets.

We emphasize that our sensors do *not* identify the individual components of a chemical mixture. Rather, the sensors recognize an overall scent. It makes no difference if the scent is a pure component or a complex multicomponent aroma, each generates unique response patterns that are recognized by ML algorithms. These properties make the sensors similar to an artificial nose or trained canines.

A. Classification Experiments

Microfabricated sensor chips with arrays of 64 sensor elements were processed using the drop casting method. The raw data for detection of VOCs, Teas, and solid explosives are similar to Figure 4. As the chemiresistors are sensitive detectors for all of the analytes studied, the main results from our studies are the classification accuracies. In addition, we tested a hypothesis about the role of chemical diversity.

A key observation of our work is that even arrays made with single types of monolayer capped nanoparticles perform well for detection and classification. This result was unexpected because we believe that chemical diversity is essential to provide robust patterns for odorant recognition. Intuitively, we expected that different sensor elements

with the same sensor material should provide redundant information not especially useful for pattern recognition, but this is not what is observed. On the contrary, we find that sensor arrays with a single type of nanoparticle can provide good classification results for pattern recognition. We attribute the good results to a *configurational diversity* that functions independently of *chemical diversity*. The mechanism of configurational diversity is discussed in more detail later.

A central feature of our "Large N" hypothesis is an expectation of improved sensor performance with greater chemical diversity. The existence of configurational diversity presents some difficulty for testing our hypothesis since both effects occur simultaneously. As part of the VOC and Tea sensing studies we designed experiments to test our hypothesis using sensor chips with both single and multiple types of monolayer capped nanoparticles. We compared performance on a per element basis. Ideally, we would have tested a series of increasing numbers of sensor materials, 1, 2, 4, 8, 16, etc. However, the spreading of microliter droplets via the drop casting method limited us to 4 different materials on a single sensor chip. Moreover, the classification accuracy is already so good with just a few types of particles that it would be difficult to see further improvements with more sensing materials. More rigorous testing of our hypothesis will require larger test sets with more chemicals, but initial results support our hypothesis. When similar sized arrays are compared, chemically diverse sets perform measurably better than a single material. The significance is that adding more sensing materials is the path to improved sensors.

i. VOC test set

A test set of 20 volatile organic chemicals (VOCs) was examined to measure performance for detecting and classifying a large set of pure compounds. These measurements also provide data for UNIFAC model development described later. Table 2 lists the 20 compounds that were tested. The major results for these measurements are the classification accuracies determined by ML processing of sensor data. We also show example confusion matrices that graphically illustrate where errors occur in the classification algorithms.

Table 2. List of VOCs detected

1	Acetone
2	Acetonitrile
3	Anisole
4	Butanol
5	Butyraldehyde
6	Cyclohexane
7	Cyclohexanone
8	Chloroform
9	Dimethylformamide
10	Dimethyl methylphosphonate
11	Dichloromethane
12	Heptane
13	Hexane
14	Isopropyl Alcohol
15	Nitrobenzene
16	N-methyl-2-pyrrolidone
17	Pentanol
18	Styrene
19	Tetrafluoroethylene
20	Toluene

The sensors for this dataset were fabricated using microscale photolithography and drop casting techniques. The sensor chip layout was designed to have 64 total devices arranged as 4 sets of 16 devices in each corner of a chip. In this way, 4 separate nanoparticle materials could be used on a single chip by drop casting particle solutions in each corner. The microliter droplets spread out to cover an area of several mm^2, so physical separation is required to avoid overlap. Each sensor chip has 64

devices, but our wiring setup currently limits us to measure only 50. Some devices are eliminated based on poor electrical characteristics yielding about 40-50 working devices for each experiment.

Two sets of ligands were investigated (Table 1). The first set of ligands were alkylamines with different chain lengths, including dodecylamine (DDA), tetradecylamine (TDA), hexadecylamine (HDA), and octadecylamine (ODA). The second set of ligands consisted of 4-(dimethylamino)pyridine (DMAP), tetradecylamine (TDA), 4-hydroxybenzoic acid (4-HBA) and 4-aminothiophenol (4-ATP). The results presented below are based on the second set. Particle sizes are in the range of 10-20 nm. The concentration of nanoparticle solutions were approximately 1.5 mg/ml. Further details on particle synthesis are available in our journal publications.

A schematic of the experiments is shown in Figure 5, which was described in the introduction. All measurements were taken at room temperature. For each of the 20 VOC analytes, six repetitions of dosing ('sniffing') were performed at four different vapor concentrations (p/p_{sat}). Baseline resistances, R_o, span a range of 1 kΩ to several MΩ. Raw data like Figure 4 are processed using peak recognition routines to produce $\Delta R/R_o$ data, which are analyzed using ML methods. All algorithms use five-fold cross-validation where datasets are split into training and test portions. The ML algorithms are trained using a 'training set' and then evaluated using a 'test set', and the process is repeated for all portioning configurations. Training produces a mathematical model that takes all the sensor readings as input and predicts the identity of unknown chemicals in the test set. Classification accuracies are based on the % of correct assignments in the test sets. We have verified that this approach is equivalent to collecting a separate dataset of unknowns and evaluating the classification accuracy with the trained algorithms. Note that for these experiments classification refers to chemical identity. 100% accuracy would mean that all unknown chemicals were correctly identified.

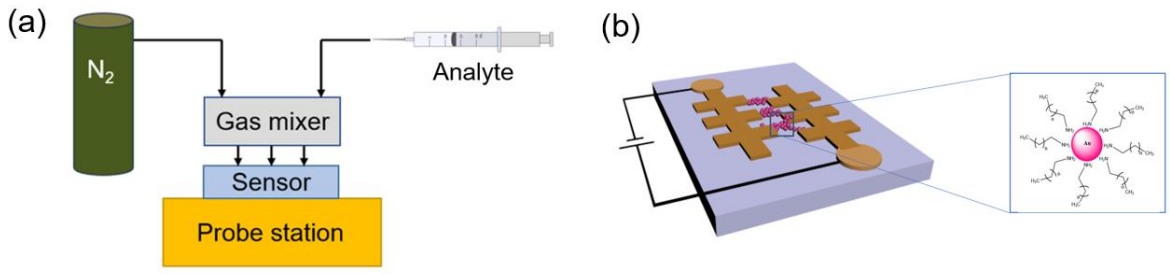

Figure 5. Schematic of experimental setup. (a) Detection of VOC analytes with chemiresistor arrays using a probe station. Saturated vapor analytes mix with dry nitrogen before delivery to a sensor. (b) Fabricated microelectrodes deposited with nanoparticles for sensing measurements.

Table 3. Classification accuracies for VOC dataset (Multi-particle chip)

	LDA	SVM	KNN	BT
Day 1				
$p/p_o = 0.25$	100	99	98	98
$p/p_o = 0.20$	98	100	94	99
$p/p_o = 0.15$	100	99	97	100
$p/p_o = 0.10$	94	95	84	98
All p/p_o	91	88	91	97
Day 45				
$p/p_o = 0.25$	98	91	94	97
$p/p_o = 0.20$	100	93	95	99
Day 90				
$p/p_o = 0.25$	96	87	94	95
$p/p_o = 0.20$	97	91	90	98
All Days				
$p/p_o = 0.20$	63	70	93	94

LDA : Linear Discriminant Analysis
SVM: Support Vector Machines
KNN: K-Nearest Neighbors
BT: Bagged Trees

The results for analysis of the full 20 VOC test set using the DMAP, TDA, 4-HBA, and 4-ATP materials set are shown in Table 3. The data are shown for different partial pressures and on different days ranging from the first testing on day 1 to 90 days after the initial testing. We show results for 4 different ML algorithms: LDA, SVM, KNN, and BT. The BT method is similar to the Random Forests (RF) method cited in other parts of this report. Examination of Day 1 data shows very high classification accuracies near 100% for all methods and partial pressures (p/p_o) > 0.10. Figure 6 shows an example of a confusion matrix for the BT method with 99% accuracy. There is only one incorrect assignment where styrene was incorrectly assigned to toluene. At the lowest concentration of 0.10, there is a drop in accuracy for three of the ML methods, but the BT results are still very good. Moreover, we expect that we can improve the results at lower concentrations by more sampling.

One of the major challenges for chemical sensing in open air environments is that not only is the chemical identity unknown, but also the concentration and quality of the odor may vary depending on distance from the source. A useful sensor has to be able to detect and identify chemicals over a range of concentrations. We have found that some ML methods are better than others for generalizing to detect chemicals at different concentrations.

Figure 7 shows an example of a discriminant plot for a subset of 6 of the 20 VOCs investigated. The plot is associated with the LDA method and gives a visual indication of the separation between different chemicals. Discriminant plots show only a fraction of the information used in classification, but they can be helpful to visualize the separation of the different chemicals as long as one keeps in mind the plots are two dimensional projections of a higher dimensional space. The discriminant plot is for a set of measurements that includes 4 different vapor concentrations. It can be seen on the plot that the six chemicals form separate groupings of data points regardless of concentration, but the separation distance is sensitive to concentration.

In practice, analyte concentrations are unknown, so sensor training must include data over a range of concentrations, which is much more challenging. Results of full analysis of all 20 VOCs at 4 concentrations is include in Table 3 in the row 'All p/p_o'. Analysis of all concentrations as a single dataset (All p/p_o) shows a drop in classification accuracy to

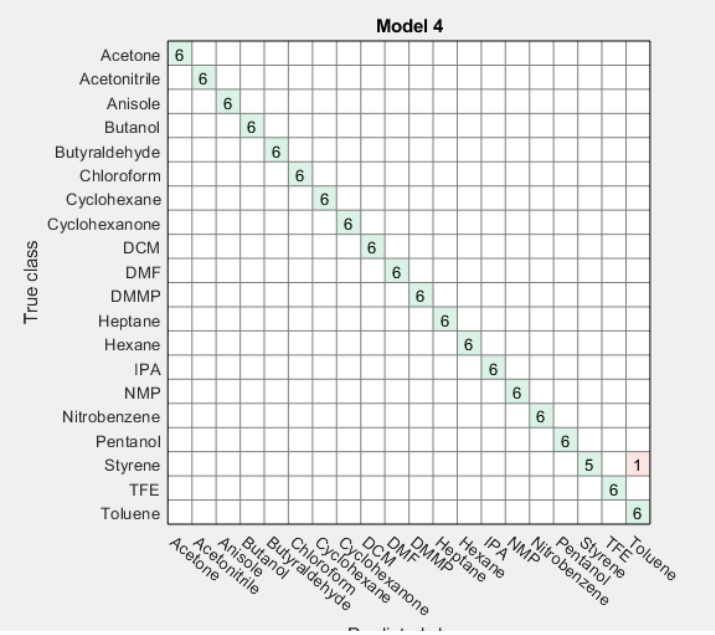

Figure 6. Confusion matrix for BT analysis on Day 1 with $p/p_o = 0.20$. (Bottom axis is 'predicted class').

about 90% for three of the ML methods, while the BT maintains impressive performance at 97%. A confusion matrix for all concentration data on Day 1 is shown in Figure 8; there are now 11 mismatches out of 480 measurements. We expect that continuous improvements in sampling, more sensor elements, and more sensor materials will provide excellent classification accuracy over a large dynamic range of concentrations. We emphasize that most studies of chemical vapor detection in the literature do not consider a range of concentrations, and these results are state-of-the-art.

We have also investigated the aging performance of our sensors over a period of 90 days. We find that individual sensor elements may have some drift of baseline R_o values, and some elements may degrade, but the overall sensor chips maintain performance. There are both increases and decreases of signal/ noise for individual sensors. Data for Day 1, 45, and 90 are included in Table 3 for two concentrations. The data show > 95% accuracy is maintained over a 90 day period using the BT method. The good performance is maintained despite the loss of 6 sensors at Day 90. The large number of sensor elements makes the overall chip robust against the loss of a few elements and we expect that designs with hundreds or thousands of sensor elements will be robust against aging.

We find that some ML methods are very good at classifying well-defined datasets, but struggle when there is more variation. Meanwhile, other ML algorithms perform slightly worse on well-defined datasets, but generalize better to larger datasets with

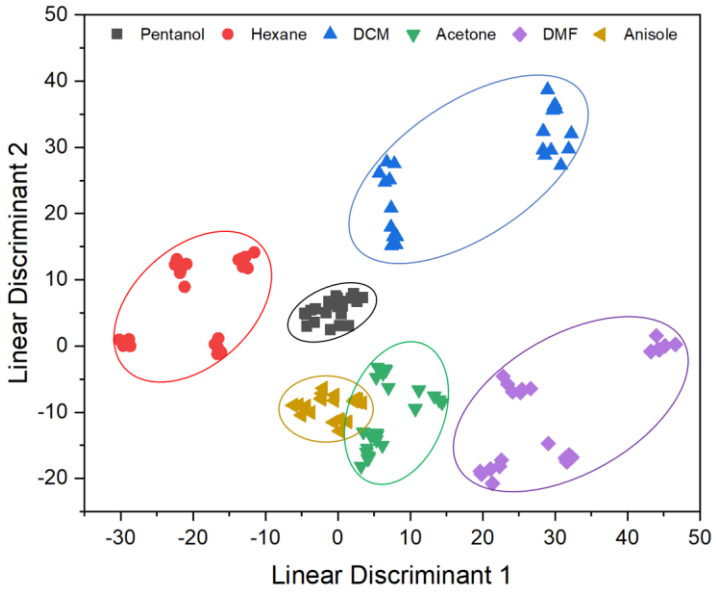

Figure 7. Discriminant plot showing the groupings of six chemicals at four different concentrations.

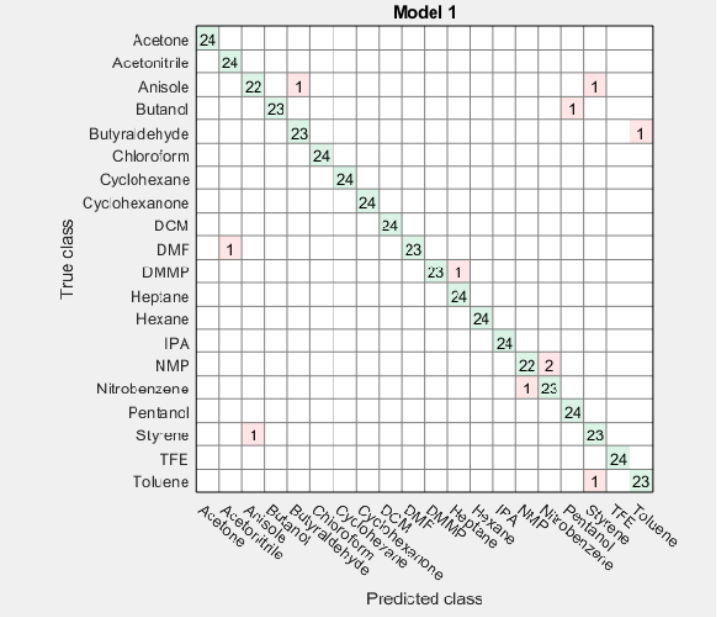

Figure 8. Confusion matrix for BT analysis on Day 1 with all concentrations (All p/p_o).

more variability. These effects can be seen in Table 3 when we analyze 'All Days' as a single data set. The LDA and SVM methods drop significantly from near 100% accuracy at Day 1 to < 70% accuracy for the 'All Days' dataset. LDA is so particular it can distinguish datasets taken on different days. By contrast, KNN and BT methods are much better at generalizing and achieve 90-95% accuracy for the 'All Day' dataset. These results are significant for practical applications where trained sensors would be implemented in the field. We note that the concept of generalization is not typically discussed in the literature and these results are state-of-the-art.

Our sensors appear to be especially well suited for the RF and BT methods, which are both based on decision trees. Results are consistently at or above 95% accuracy, and the method generalizes well to different concentrations and sensor aging. The results shown here for VOCs and the further results below for Teas are very promising for a new class of chemical sensors that can detect and identify a large number of chemicals over a useful dynamic range of concentration. These sensors could find use for detection of precursor chemicals as well as explosives.

ii. Tea set

We have applied our sensor chips to detect and classify complex, multicomponent odors using a set of 39 commercial Teas. The Teas include several green, black, and herbal varieties. The overall approach and methods are similar to the VOC study above. This work has been recently published in a special issue dedicated to nanosensors. The article includes details on the types of Teas tested. Therefore, we do not reproduce all of the data here, but focus on the main results.

Tables 4 and 5 summarize the main results for the Tea experiments. Table 4 lists classification accuracies for a sensor chip using four different sensor materials. The data are analyzed as one group of black and green teas, and a separate group of herbal teas. The classification data are listed for a sensor chip with all materials together, as well as subsets of each sensor material analyzed separately. The overall sensor chip with all

Table 4. Classification accuracy for different sensor materials

AuNP	Number of Working Devices	Accuracy (%)	
		Black and Green Tea	Herbal Tea
DMAP	10	97.1	75.0
ODA	11	77.9	77.8
MPA	8	52.9	52.8
ATP	9	53.8	43.8
Overall	38	100	97.7

four materials and all 38 sensor elements performs better than any individual material, but direct comparison is unfair since the overall chip has nearly four times as many elements. For a more balanced comparison, two devices of each sensing material (nanoparticles) were randomly selected to create groupings of eight multi-particle sensing elements for comparison with single particle data on an equal number basis (i.e. eight multi-particle vs. eight single particle). The classification results for the multi-particle set are 91.4 $\pm$ 3.3 % accuracy for black and green teas, and 88.6 $\pm$ 3.7 for herbal teas, which should be compared with the four separate materials. Although the DMAP particles perform very well for the black and green teas (97%), the performance for the herbal teas (75%) is significantly less than for the multi-particle arrangement. The combination of the four types of particles performs better overall than any of the single types of particles, which supports our hypothesis that more chemical diversity enhances sensor performance. We expect that adding even more elements and sensor chemistries will further improve overall performance. However, larger and more challenging test sets may be needed to more clearly demonstrate the advantages of more materials.

The data in Table 4 also demonstrate the structural diversity effects discovered in this work. We observe that the classification accuracy of DMAP particles alone for the black and green teas is 97%, which is unexpectedly good. Figure 9 shows an example of a separate experiment using a chip with 42 DMAP sensor elements to detect 21 Teas. We analyze the classification accuracy as a function of the number of sensor elements using three ML methods: LDA, KNN, and BT. Qualitatively, the methods all perform similarly, starting with a low accuracy for a single sensor, rising rapidly for 1-10 elements, plateau for 10-20, and then a gradual increase to 100%

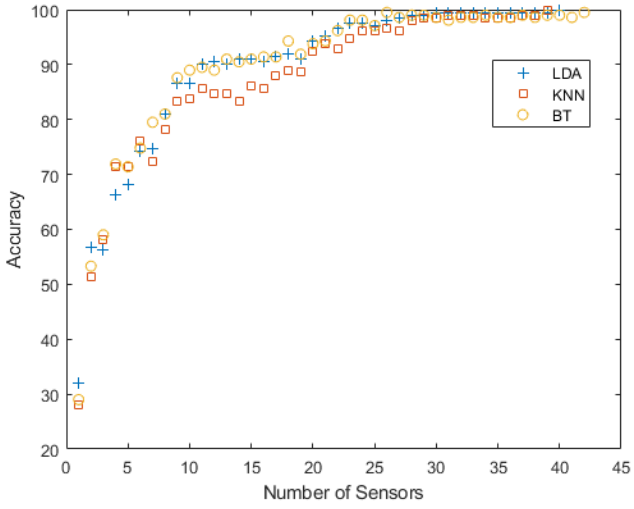

Figure 9. Classification accuracy vs. number of sensors on a chip for DMAP particles and 21 Teas.

accuracy for nearly all 42 sensor elements. There are several interesting features in this data. For one, we see that the increase of accuracy with the number of sensors elements is not smooth. Some sensors make no difference, and some cause a slight drop in accuracy. The data also demonstrate that beyond 20-25 sensor elements, the data are robust against the loss of one or even several elements, which was also seen in the VOC data for the 90 day experiments. Some elements appear redundant, but there is a steady increase of information content with increasing numbers of sensor elements that is unexpected based on simple chemistry arguments. The explanation is configurational diversity, which we discuss later.

Table 5. Accuracy over a 5 day period

Day	LDA (%)	SVM (%)	KNN (%)	RF (%)
1	100	97.1	93.3	99.7
2	96.2	97.1	98.1	99.7
3	90.4	88.5	87.5	98.6
4	86.5	91.3	88.5	98.9
5	97.1	98.1	97.1	99.8

Table 5 shows results for a multiday experiment to test sensor stability. Sensors were tested on the black and green tea set over five sequential days, and the classification accuracy was determined each day. We found a gradual decrease in the accuracy on days 2 and 3 followed by recovery on days 4 and 5. The dip is smallest for the RF method where accuracy remains high on all days, but it follows the same qualitative trend as the other methods with an apparent dip at day 3. We believe this drop and subsequent recovery is associated with drift in the baseline R_o values due to gradual room temperature rearrangements of the nanoparticles, and/or burn-in from the testing. The baseline drift (not shown) appears to correlate with classification accuracy. Baseline R_o values decrease from day 1 to day 3, but then stabilize.

Overall, the Tea results show that our sensors are capable of detecting and classifying complex odors with high accuracy. The overall classification accuracy for the full set of 39 black, green, and herbal teas is 98.6%. The test set of 39 distinct odors (aromas) is the largest that we have seen in the literature. We believe that larger test sets and higher performance can be achieved by expanding to more sensor devices and more sensing materials.

B. Testing of Explosives and Related Materials

In addition to our work with large test sets of VOCs and Teas, we have also investigated detection and classification of materials more directly relevant to explosives detection. Table 6 gives a list of some of the chemicals of interest for explosives detection. Materials that we have studied are highlighted in yellow. Detection of 2,4 DNT was demonstrated in Figure 4 above, and acetone, cyclohexanone, and nitrobenzene were included in our VOC study. Figure 10 shows data for ammonium nitrate (AN) detection, similar to the DNT plot, but the AN data have been processed to $\Delta R/R_o$. The 16 sensors are a subset of 64 devices on a single sensor chip. The spikes correspond to pulses ('sniffs') of diluted AN vapor, and the responses for all sensor elements are simultaneous. These data show

Table 6. Explosives and related materials

Nitro-aromatics
Nitrobenzene (NB)
Dinitrobenzene (DNB)
Trinitrobenzene (TNB)
Nitrotoluene (NT)
2,4 & 2,6 Dinitrotoluene (DNT)
Trinitrotoluene (TNT)
Picric acid
DMNB
EGDN
Nitroglycerin
Ammonium Nitrate
N_2O
Potassium Nitrate
Potassium perchlorate
Peroxides
acetone
TATP, DADP
HMTD
Hydrogen Peroxide
HMX
RDX
cyclohexanone
PETN
Tetryl
Composites: amatol; comp B; semtex; C4; detasheet; gun powder; fireworks; etc.

that our sensors respond quickly and sensitively to explosives related materials that are solids at room temperature.

We have also used AN to investigate the detection speed of our nanosensors. Figure 11 highlights rapid detection of AN with a time constant of 100 msec. The square wave form of the signal is unique to the nanoscale sensors and reflects ultrafast saturation. The time constant is limited by the experimental setup and we expect that faster response speeds can be achieved with more work. As discussed in the introduction, rapid response rates benefit from nanoscale sensors with low capacitance and fast mass transport compared to larger devices.

The above experiments were done using commercial chemicals, but we have also analyzed standard samples used for K-9 training. K-9 NESTT training aids were obtained from Ray Allen K9 supplies. The kits include TNT, RDX, PETN, oxidizers, and a silica distractor. There was a delay in obtaining the samples due to regulations, so that a full analysis was not performed. Preliminary results achieved 100% accuracy for detection and classification of TNT samples compared with the silica distractor. The experiments demonstrate robust detection of TNT vapor at room temperature. Future work will study all materials in the kit.

3. Modeling

We have pursued two different modeling approaches to gain deeper insight into how our sensors function and how to design for improvement. As should be evident from the discussion above, there are two key features of our sensors that provide capability for detection and classification. These features are chemical diversity and configurational diversity. A UNIFAC model was developed to improve our understanding of chemical diversity, and a resistor network model was created to investigate configurational diversity.

A. UNIFAC Model

Nanoparticle chemiresistors sense vapor analytes through a mechanism that involves sorption of vapors into sensing materials as represented in equation (2).

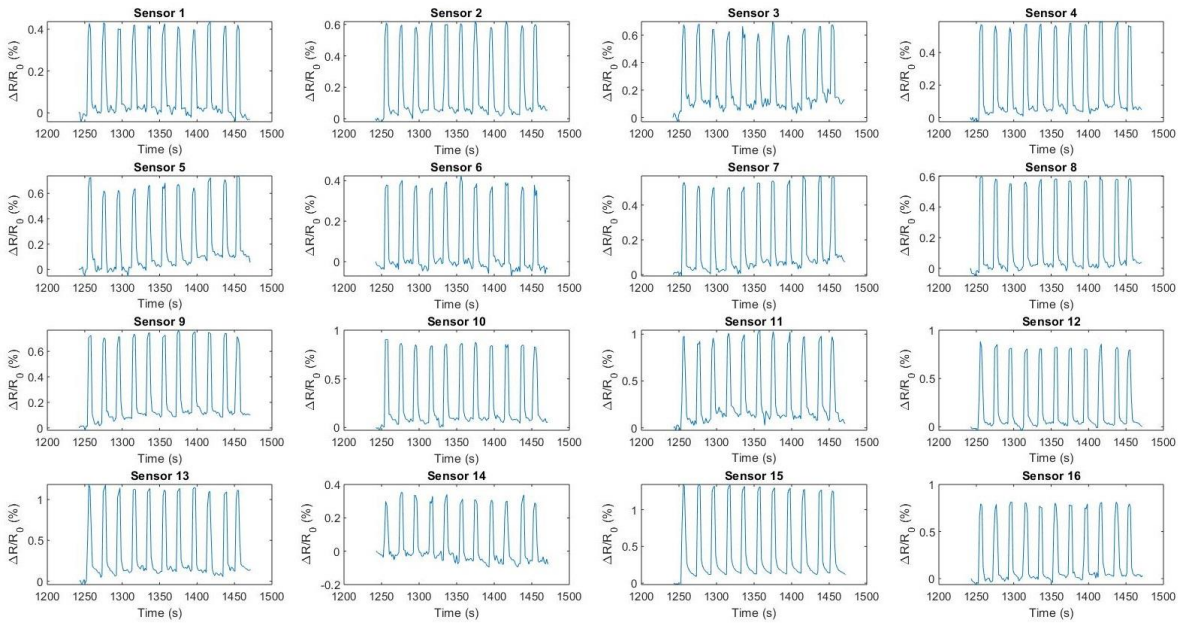

Figure 10. Processed data for a subset of 16 out of 64 sensor elements that simultaneously detect ammonium nitrate. Each peak is a few second pulse of diluted vapor.

$$\text{Analyte (g)} \leftrightarrow \text{Analyte (s)} \qquad (2)$$

Equation (2) represents that analytes partition from the gas phase (g) into the solid (sorbed) phase (s). For fast molecular transport processes, analytes will partition into the solid layers until equilibrium is established. At equilibrium the rates of partitioning into and out-of the sensing materials become equal, and a steady amount of analyte in the sensing materials is reached. The equilibrium ratio is only a function of temperature for ideal gases, and can be represented as a partition coefficient, K(T). Accordingly, the concentration of analytes that partition into sensing materials depends on the partition coefficients and the concentrations in the gas phase (see equation (5) below). Generally, K values are >> 1, and the volume concentration of analytes is much higher in sensing materials than in the gas phase. The absolute amount of analytes that partition depends also on the volume of sensing materials, which favors nanoscale sensors for high sensitivity. In the discussion below, we assume that molecular transport processes are sufficiently rapid so that our sensors achieve equilibrium concentrations as per equation (2) above. The assumption allows us to treat the process according to established principles of equilibrium thermodynamics to estimate K values. The assumption of fast mass transport is supported by time dependent sensing data that exhibit steady responses that track gas phase concentrations.

As introduced earlier, equation (1) provides a general mechanism for how nanoparticle-based chemiresistors function. The most important factor is $\Delta\delta$, which is a change of particle - particle distance due to swelling. Swelling occurs when vapor analytes partition from the gas phase into sensing materials that make up the sensor elements. Rational

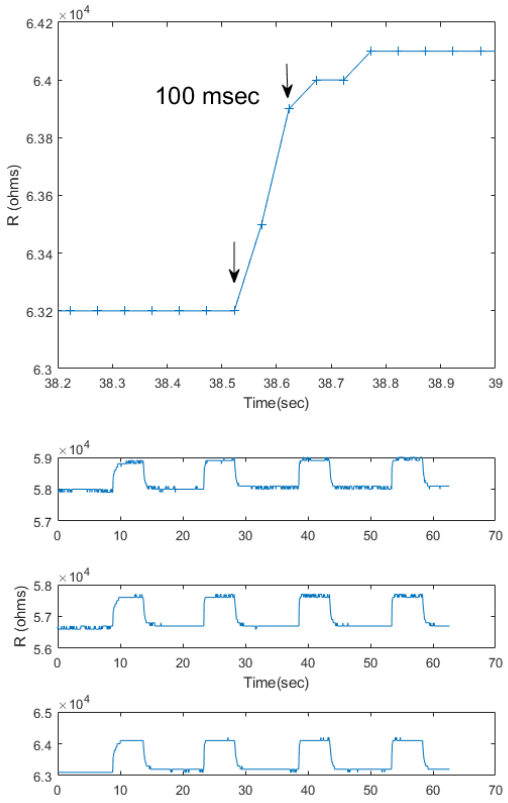

Figure 11. Sample data for rapid detection of ammonium nitrate with 100 msec response.

design of sensor materials could be accomplished if the partition values could be predicted from chemical models.

We have initiated a new approach to sensor modeling using the UNIFAC method as a chemical model to predict sensor responses. To the best of our knowledge we are the first to build quantitative, predictive models for chemical sensor development. Here, we describe our approach and show preliminary work that has been done to validate the model.

UNIFAC is a theoretical method used to model the chemical properties of a large number of chemical compounds (> 20,000). The method is used extensively in the chemical industry for modeling chemical separations processes of complex mixtures. The theory behind UNIFAC is to treat molecular scale interactions as combinations of pair interactions between all functional groups of molecules. The method began as academic research in the 1970s, but is now maintained by an industry group, The UNIFAC Consortium (http://unifac.ddbst.de/unifac_.html). The group sells software codes that allow users to calculate various molecular properties, including activity coefficients for vapor / liquid systems. Figure 12 illustrates a graphical representation of the available parameters for different chemical groups. Only molecules with a complete set of parameters (filled squares) can be modeled. As can be seen in the chart, most parameters are incomplete or missing. As a result, the diversity of chemicals we can predict is limited, which is unfortunate for sensors modeling. Nonetheless, a large number of chemical compounds can be modeled (> 20,000) using the available parameters, and UNIFAC is the only available predictive chemical method with such a large database.

We have developed an approach to use UNIFAC to calculate activity coefficients and predict sensor responses for different combinations of vapor analytes and sensor materials. As described in the introduction, our sensor materials are core-shell assemblies of metallic nanoparticles (core) and organic layers (shell). The organic layers are immobilized onto metallic (gold or palladium) particle surfaces via covalent bonds through thiol or amine chemistries. Unfortunately, UNIFAC does not include a complete set of parameters for either thiol or amine chemistry; and, of course, it does not account for the metallic nanoparticles. Therefore, we have mapped our problem onto a simpler, solvable problem.

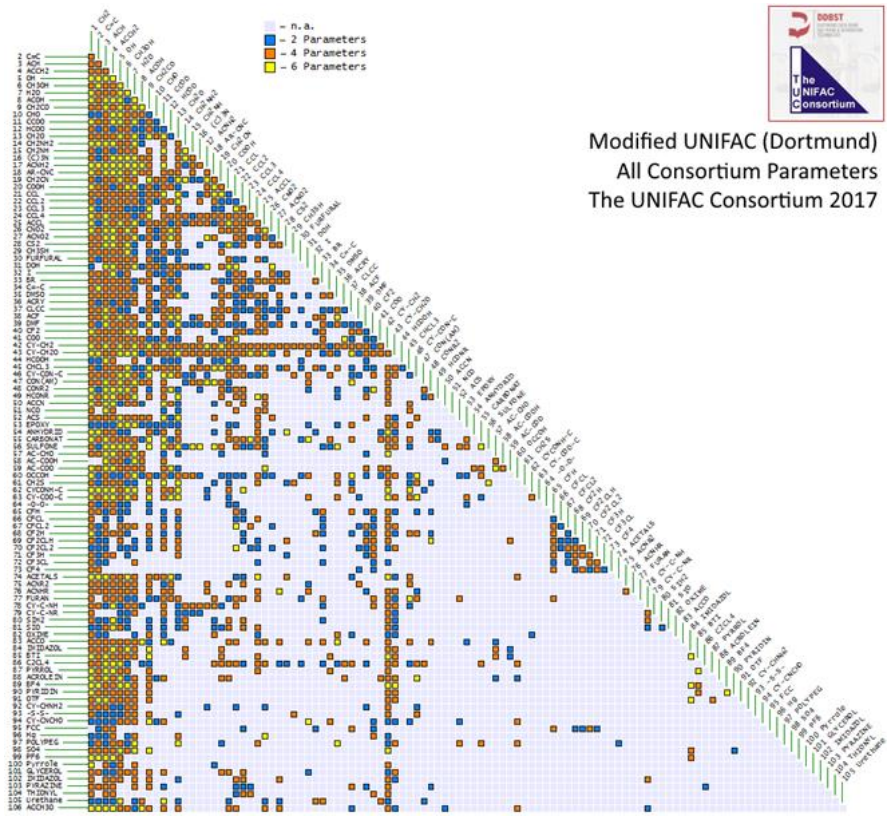

Figure 12. UNIFAC parameter set.

The first assumption is that the metallic cores do not play a significant role in chemical sensing. This is reasonable since the metallic cores are coated with a dense layer of the sensing materials (shell layers) and there should not be much free surface area of the metallic cores exposed. Thus, we remove the effects of the metallic cores from the model. Next, we make a similar assumption for the amine and thiol groups that anchor monolayers to the metallic cores. These groups are pinned at the metal interface and do not have the same flexibility as the rest of the molecular chain. Moreover, they are a small fraction of the full organic monolayers, and thus may play a small role in vapor sorption. After removal of the metal core and anchoring groups from consideration, we are left with the molecular structure of the organic shell layers. For many sensor materials, the organic shell layers can be modeled using available UNIFAC parameters. As an example, a shell material like octanethiol would be modeled as octane, dodecylamine is modeled as dodecane, etc. In this way, each of the sensor materials in Table 1 can be mapped onto a simpler chemistry.

The last assumption is that the organic molecules that make up the shell layers can be modeled as a liquid environment not too different from a normal liquid represented by the UNIFAC parameters for that material. This last assumption seems reasonable on a chemical basis, but may account for differences between experiment and calculated data.

The net result of these assumptions is that we model analyte/ sensor material interactions as a vapor/ liquid equilibrium problem well known in thermodynamics.

In our model, activity coefficients are calculated at the infinite dilution limit for pairs of analytes and sensing materials. The partial pressures of vapor analytes are known from experiment design and relate to the vapor concentrations via the ideal gas law as shown in equation (3).

$$P_i = C_i RT \tag{3}$$

Where P_i is analyte partial pressure in atmospheres [atm], C_i is concentration in [moles/liter], R is the gas constant, and T is absolute temperature [K]. Analyte partial pressures, P_i, are used along with UNIFAC computed activity coefficients γ_i, and saturation pressures $P_{i,sat}$, in Raoult's Law to calculate the mole fractions x_i, as in equation (4).

$$P_i = \gamma x_i P_i^{SAT} \tag{4}$$

The mole fraction x_i, is the amount of vapor analyte that partitions/ sorbs into the sensing medium at equilibrium. Saturation vapor pressure data $P_{i,sat}$, are found in databases such as the CRC Handbook of Chemistry for pure compounds. All of the molecular scale chemical interactions are contained in the activity coefficient. For a typical experiment, $P_i/P_{i,sat}$ ranges from 0.001 to 0.1. Equation (4) is solved for x_i to predict the amount of material detected in an experiment. We see that the mole fraction is inversely proportional to the activity coefficient. Large activity coefficients indicate incompatible chemicals that do not mix, while activity coefficients near 1.0 indicate ideal mixing. Thus, a large range of activity coefficients is desirable to produce feature rich patterns for classification. A large range of activity coefficients can be realized with many different sensor materials.

With the mole fraction x_i computed, the concentration of analytes in the sorbent phases (sensor materials) can be calculated using the density and molecular weight of the analytes. The concentrations of analyte in the gas and condensed phases are related by the equilibrium constant, equation (5).

$$K = \frac{C_{sorbent}}{C_{vapor}} \tag{5}$$

The equilibrium constant (partition coefficient) is a measure of the strength of the chemical interaction between analyte and sorbent such that high partition coefficient values indicate significant vapor sorption for a small concentration in the gas phase (C_{vapor}). Typical values of K for gas-solid systems like ours range from 10^3 to 10^6. The net result of equations (3) - (5) is the ability to predict $C_{sorbent}$, which are the amounts of analytes that partition into sensor materials. Calculations can be done for any materials that can be modeled using the UNIFAC methods and the predictions can be used to design sensor arrays for different analytes or to optimize separations with known interferents.

Further progress in our model requires a connection between the chemical models for $C_{sorbent}$ values and a physical model for device electrical response. As discussed above, equation (1) shows that the major effects of analyte partitioning is to cause swelling of particle networks, thus displacing particles from their normal positions and modifying the electrical resistances of particle - particle connections. The logic for the physical model is lengthy and not reproduced here, but the qualitative idea is very simple. We model the swelling effect as the addition of the molar volume of analyte molecules sorbed into the sensing layers. The volume expansion is computed from the analyte concentration, $C_{sorbent}$, and its pure component molar volume. Linear expansion of the network, $\Delta\delta$, is then computed as the cube root of the volume expansion. Alternatively, we could take the 1/n root where n is a parameter. The rationale behind allowing n to vary from 3 is that the volume expansion may not be uniform in all particle networks. Our model can be equally applied for pure materials or chemical mixtures, as long as UNIFAC parameters are available. Here, we use the pure chemicals from our VOC measurements (Table 2) for validation studies.

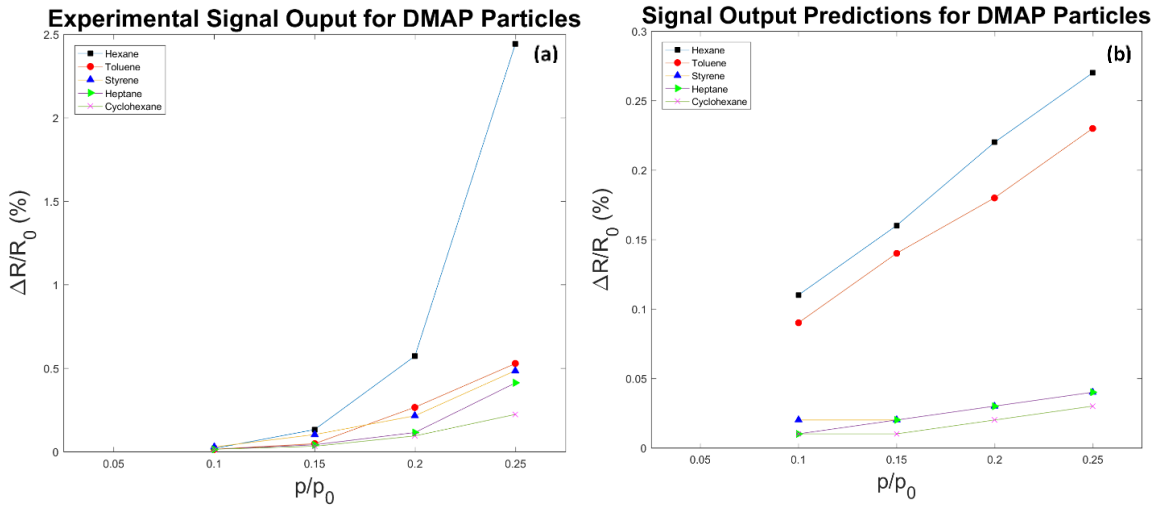

Figure 13: (a) Experimental and (b) predicted $\frac{\Delta R}{R}$ signal outputs for DMAP particles across four different $\frac{P}{P_0}$ concentrations. The tested VOCs are hexane, toluene, styrene, heptane, and cyclohexane.

Table 7. Predictions vs. Experiment for DMAP particles

Partition Coefficient (K) Ordering	Partition Coefficient (K)	Predicted ΔR/R Ordering	Experimental ΔR/R Ordering
1. Styrene	1.01×10^4	1. Hexane	1. Hexane
2. Toluene	2.87×10^3	2. Toluene	2. Toluene
3. Cyclohexane	178	3. Styrene	3. Styrene
4. Heptane	172	4. Heptane	4. Heptane
5. Hexane	67.5	5. Cyclohexane	5. Cyclohexane

A subset of vapor analytes and sensing materials was used to validate our UNIFAC model. Results from the model are compared with experiments in Figure 13. Data are shown for hexane, toluene, styrene, heptane, and cyclohexane interacting with DMAP particles. The experimental data are normally linear like the simulated data, but this particular sensor chip has some atypical upward curvature. Nonetheless, the data are useful for model validation. The main interest is to compare the relative ordering of the different analytes for experiment and theory. Table 7 summarizes the data and includes UNIFAC calculated partition coefficients. The model and experimental ordering of the $\Delta R/R_o$ responses are the same, which is a very nice result. It is interesting that the model does not follow the ordering of the partition coefficients. It would seem that although K is an important component to the model, other factors such as vapor pressure and molar volume are also factors in the model. Although the predicted chemical ordering is correct, the calculated $\Delta R/R_o$ are about a factor of ten less than experiment. More work is needed to investigate the origin of the under predicted signal intensity.

Table 8. Predictions vs. Experiment for MPA particles

Partition Coefficient (K) Ordering	Partition Coefficient (K)	Predicted ΔR/R Ordering	Experimental ΔR/R Ordering	Experimental ΔR/R (%)
1. Butanol	2.24×10^4	1. Hexane	1. Hexane	2.49
2. Acetone	1.10×10^3	2. Butanol	2. Butanol	2.23
3. Hexane	315	3. Acetone	3. Acetone	1.81

A second validation experiment was done using a different sensor material, MPA. Table 8 shows these results for a small set of three vapors. The results are similar to the DMAP experiments. The experiment and predicted chemical orderings match, but the predicted signal intensities are again too low (not shown). As with Table 7, $\Delta R/R_o$ predictions are more complex than a simple ordering of partition coefficient values, which demonstrates the importance of other parameters in the model. Overall, the validation studies show a good match between experiment and theory that supports our UNIFAC approach. More work is needed to determine the broader applicability of the model. Cases that don't fit the model may teach us new things about other chemical effects operating at the nanoscale.

We have also used our UNIFAC model to perform several computational experiments to investigate how our sensors would perform if we had more sensing materials. These hypothetical computer experiments are a test for the 'Large N' hypothesis that underlies our approach. We find that simulating sensor arrays with 150 materials enables robust detection and identification of over 100 different chemicals. Further, we believe the chemical identification list could be extended to thousands of chemicals. It is encouraging that our models show that very effective sensors can be designed even with the limited types of chemistries that can be modeled with UNIFAC. Overall, we find strong theoretical evidence for the benefits of chemical diversity in sensing materials. Future work needs to investigate how large arrays of chemically diverse sensing materials can be fabricated.

B. Nanoparticle Networks

One of the main findings of the research project was significant variability between sensor responses for nominally identical sensors integrated on a single chip. For a given sensor material and a given vapor analyte, one may have expected similar responses from neighboring sensors, within measurement repeatability. However, we observe significant variability between similar sensors that cannot be understood from simple chemistry arguments. Table 9 shows an example of the variability for 37 sensors detecting nitrobenzene using TDA particles. The $\Delta R/R_o$ values range from a minimum of 3.48% to a maximum of 7.93% with an average of 5.56%. All sensor elements have the same type of nanoparticle sensor materials, and the range of responses is not expected based on pure chemistry considerations, which would predict a single value. For the ML algorithms, the variability adds to the information content of the sensor array and enhances overall performance. Though we emphasize a need for chemical diversity as well, configurational diversity means that even sensor chips with a single type of particle can perform quite well as detectors.

Previous studies might have attributed variations between sensors to inhomogeneous vapor concentrations between neighboring sensors separated by relatively large distances of several mm, but our sensors are very close together with separation distances of only a few microns. Therefore, we do not believe that significant concentration gradients are present. Some variability could originate from non-uniformity of the monolayer coated particles. For example, there are particle size distributions and there are different particle shapes in a batch of nanoparticles. However, we think it more likely that particle arrangements themselves contribute to device

Table 9. Example of experimental data for nitrobenzene detection with TDA particles

Sensor	$\Delta R/R_o$ (%)
1	3.48
2	4.17
3	5.09
4	4.59
5	4.18
6	4.39
7	4.57
8	5.17
9	5.42
10	4.47
11	5.35
12	4.92
13	4.80
14	4.68
15	6.94
16	5.43
17	5.30
18	4.34
19	4.62
20	6.99
21	5.08
22	5.75
23	6.80
24	6.24
25	5.06
26	6.26
27	6.97
28	6.65
29	7.83
30	6.58
31	5.92
32	6.08
33	6.15
34	6.23
35	5.79
36	5.57
37	7.93
Mean	*5.56*
STD	*1.06*
Range	*4.44*
Min	*3.48*
Max	*7.93*

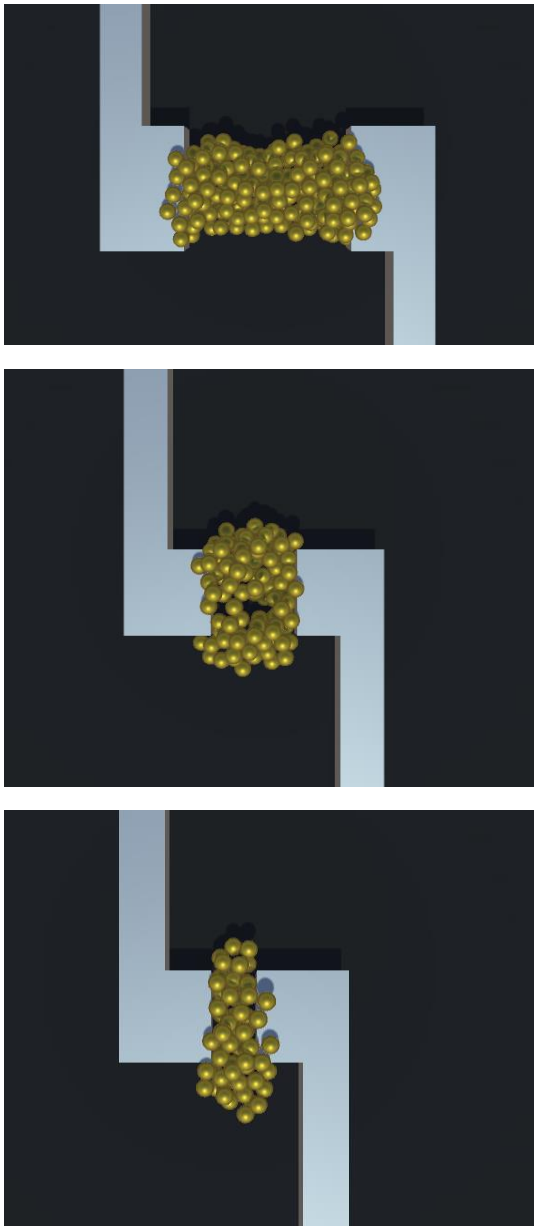

Figure 14. Images of particle assemblies analyzed in this work. Particles are 20 nm in size, electrode spacing ranges 50-200 nm. Top to bottom are labeled as Networks A, B, & C.

to device variability. Therefore, we have investigated how particle organization may contribute to response variability.

The electrical conductivity of NP films is due to electron tunneling between neighboring nanoparticles. The overall resistance of NP networks depends on the arrangements of particles, including disorder. Types of disorder include variations in the network topology, distributions of nanoparticle sizes, and variations of particle - particle spacing. Topological variation means that no two sensor elements are the same, and differences are likely to be greater for small sensors. Variations of particle arrangements means that nanoparticle films behave as random networks of widely varying tunnel conductance. Because of the exponential characteristics of the electron tunneling transport mechanism, even small variations of particle spacing can yield orders of magnitude difference in the conductance between particles.

We have developed a numerical model to simulate the sensing characteristics of randomly assembled particle networks to better understand the origins of configurational diversity. We have created a software package with a graphical user interface to assemble nanoparticles into networks by a mouse-controlled point and click builder. We use the software to create nanoparticle networks like those shown in Figure 1. Network models with several hundred nanoparticles have been assembled. Figure 14 shows a set of three different particle arrangements that were investigated in this work. There are infinite possibilities, but these three were chosen to be representative of the different types of particle arrangements that could be present in a working sensor device. The particle assemblies are different in the number of series and parallel connections, the electrode - electrode width and distance, as well as the total number of particles. The height of the electrodes and the particle sizes were fixed to the same values as experiments. The connectivity between the particles is random, and they are not close packed or stacked in any

particular arrangements. Once physical models of the networks are configured, a separate software code assigns resistances to each of the nanoparticle junctions and computes the overall network resistance. The problem is similar to solving 3 dimensional networks of resistors.

Table 10. Sensor simulations for various models. Values are averaged over 10 runs each

Model	Network (Figure 14)	Initial Resistance (R_o) (Ohms)	$\Delta R/R_o$ (%)
1	A	583580	5.0
	B	429080	5.0
	C	625006	5.0
2	A	1365400	5.11
	B	941530	5.03
	C	642310	5.44
3	A	307000	8.16
	B	202000	8.19
	C	160000	8.50
4	A	452400	5.60
	B	370800	7.13
	C	234290	7.68

We used the network configurations of Figure 14 to test several hypotheses, several of which were not supported by the models. Here we describe these hypotheses as models 1 through 4. For each particle arrangement, we calculate an overall network resistance before and after a simulated sensing experiment. The models all use the same approach to calculate the overall resistances of the particle networks, but differ in how the electrical properties of the individual particle junctions change during a sensing experiment.

Each particle – particle junction is modeled as a resistor, and the overall network resistance is calculated based on Kirchoff's law and solving for the current and voltage at each junction. During a simulated sensing experiment, the resistance of each particle – particle junction is modified according to a model for how analytes might affect the junction. In general, analyte partitioning into the sensing materials is expected to swell particle – particle junctions and increase resistance. The goal of the simulations is to determine whether the models can reproduce the variability between sensor elements seen in experiments. To avoid confusion, we will use capital R for the overall network resistance (all particles) and lower case r for individual particle - particle junctions, both symbols refer to electrical resistance. Results from the different models are summarized in Table 10. Each entry is an average over 10 simulations.

The first hypothesis (Model 1) is that different network configurations with different baseline resistances might have different overall $\Delta R/R_o$ responses even for the same $\Delta r/r_o$ of each particle - particle junction. The hypothesis was tested by computing the overall $\Delta R/R_o$ of the three networks in Figure 14 while keeping the modulation of each junction the same ($\Delta r/r_o$ = constant). The r_o values for each of the 100s of particle - particle junctions were randomly assigned according to a Gaussian distribution. The center and width of the Gaussian distribution were chosen to yield overall network resistances R_o similar to experimental measurements, with baseline resistance values near 0.1 - 1 MΩ. Results from the simulations are shown in Table 10 for model 1. We observe that the

overall network $\Delta R/R_o$ was similar to the junction $\Delta r/r_o$ (5%), even for networks with different baseline R_o values. Thus, model 1 could not reproduce experimental observations like Table 9, where different sensors produce different $\Delta R/R_o$ values for the same analyte/ sensor material combinations. Model 1 results can be understood from simple arguments using series and parallel resistors, but it was not obvious that such a simple result would be obtained for the complicated arrangements in Figure 14.

The next hypothesis with Model 2 is similar to Model 1, but we relax the assumption that each particle - particle junction undergoes the same Δr change. In addition to allowing the resistances r_o to vary as a distribution, we allow Δr to also vary as a Gaussian distribution. Now, each of the many particle – particle junctions has different r_o and Δr values, randomly assigned. The hypothesis is that different sensor elements could have different overall $\Delta R/R_o$ due to random variations of the Δr of each component junction. Justification for this model is that each junction could have a different swelling efficiency from the different local properties of the organic shell layers and particle distances. As shown in Table 10, results of this model do produce some variations of $\Delta R/R_o$ from sensor to sensor for different particle arrangements. However, the variations are small and do not render the magnitudes seen in experiments. It is apparent that randomly assigned Gaussian distributions of $\Delta r/r_o$ get averaged over a large enough number of particle junctions to smooth out the variations between different particle assemblies. We conclude that random variations of r_o and/ or Δr are not sufficient to explain experimental results, even for widely different particle arrangements like those in Figure 14.

The next model, Model 3, uses distance distributions instead of assigning junction resistance values. Distances between particles are more fundamental and physically represent the space occupied by the organic layers of the monolayer capped nanoparticles. Distances are related to resistances through the probability for charge carriers (electrons) to hop between particles via quantum mechanical tunneling. We use the simplest tunneling expression from Simmons' derivation for a rectangular tunnel barrier at low voltages:

$$J = 3.16x10^{10}\varphi^{\frac{1}{2}}\left(\frac{V}{s}\right)\exp(-1.025 * s * \varphi^{\frac{1}{2}}) \qquad (6)$$

, where φ is electronic barrier height, V is applied voltage, and s is particle - particle distance [J.G. Simmons, Journal of Applied Physics, v. 34 (6) p. 1793 (1963)]. The barrier height is an unknown parameter that we model as 1 eV. Higher/ lower barrier heights would shift our distances to smaller/ larger values, but do not change the qualitative trends or conclusions. The equation does not include charging effects, but these are not important for our networks since our particles are relatively large (20 nm) and the organic matrix is fixed (same dielectric constant). We have verified that particle – particle voltage drops are small, so that the assumption of low voltage is fulfilled. Equation (6) gives a current density (Amps/cm^2) and needs to be multiplied by an area to calculate current. Keeping in mind that the particles are not truly spheres, we choose a small patch of a sphere spanning a polar angle of 24 degrees as representative of the interfacial area between neighboring spheres. The resistance at each junction is determined from the

current density and assumed area. In this way, particle – particle distances are converted into resistances. The advantages of this approach is that we can compare it more directly with our microscopy images.

Model 3 is similar to Model 2 except that distributions are for distances instead of resistances. Gaussian distributions of both particle – particle distances (s) and analyte induced variations (Δs) simulates sensing experiments. Parameters were chosen as 0.7 nm and 0.001 nm for the mean s and Δs, respectively, to give baseline values (R_o) and responses ($\Delta R/R_o$) consistent with experiments. The average particle spacing of 0.7 nm is somewhat smaller than expected based on the physical length of the organic monolayers, but is within reasonable bounds. The small spacing is consistent with inter-digitation of monolayers on neighboring particles, which has been observed in the literature. Here, inter-digitation means that the organic monolayers on adjacent particles interpenetrate each other so that the distance between particles is significantly less than the sum of the two monolayer thicknesses. The small mean spacing may also indicate that monolayers are bent and disordered, not fully extended molecules. The distributed s values are calculated using a truncated Gaussian distribution to avoid short circuits or negative distance values.

Results for Model 3 are included in Table 10. Similar to Model 2, baseline R_o values differ for the three particle networks, but the $\Delta R/R_o$ values are similar for all three networks. There is a slight trend to larger $\Delta R/R_o$ with lower baseline (R_o) resistance, but the variations are small compared to experimental variation (Table 9). We observe that calculations of resistances through tunneling equations using distributions of s and Δs are not functionally different than distributions of resistances like Model 2. Neither model explains significant differences for different particle networks.

Based on results from Models 1-3, we conclude that simple random variation of the properties of particle - particle junctions cannot explain experimental observations. We conclude that there must be systematic features of particle networks that cause sensing variations. Inspection of high resolution microscopy images like Figure 1 shows that particle networks differ in how particles clump and connect to electrodes. Some particle assemblies have three dimensional shapes and some have more two dimensional character. Some are thick and spatially condensed over the electrodes and some have extended strings of particles or narrow constrictions between clumps. The networks have different numbers of particles and differ in the relative content of series and parallel arrangements.

Based on the above features of particle networks, we hypothesize that local configurations around any given particle may influence the local interactions with analytes and the extent of swelling. This heterogeneity of the local environment may influence resistance modulation during sensing. The heterogeneity may depend on the topology of the particle networks in a non-random way that Models 1-3 do not capture. To model these network topology effects, we propose that local swelling (Δs) is inversely proportional to particle connectivity. Particles buried under other particles with many neighbors may be constrained to have small swelling responses, while less connected

particles at surfaces, edges, or linear configurations are less constrained and swell to a greater extent. The dependence of swelling on the local environment introduces a systematic effect (not random) that depends on how particles are configured in a network. Networks with dense arrangements will respond differently than sparsely connected particles.

Model 4 incorporates configurational information to the distribution of $\Delta r/r_o$ values. Whereas Model 2 uses a Gaussian distribution of $\Delta r/r_o$ values randomly assigned to different particle - particle junctions, Model 4 assigns $\Delta r/r_o$ values based on the local environment around each particle. Like Model 2, both r_o and Δr are randomly assigned according to a Gaussian distribution, but Model 4 then uses the local configuration around each particle to modify Δr for each junction. The local configuration is quantified by counting neighbors around each junction. In this way, the swelling efficiency depends on the local environment. We make the assumption that swelling is greater for lower coordinated particles near edges and less for highly coordinated particles buried into a bulk like environment. The assumption is based on intuition that particles with more free volume can expand more easily than highly constrained particles.

With configurational effects included in the model, we see a wider span of $\Delta R/R_o$ values ranging from 5.6 to 7.7 %, which more closely matches experimental data. The trend to larger $\Delta R/R_o$ for configuration C can be rationalized based on the larger edge to bulk ratio, where edge particles are freer to expand and yield a higher response. We can now understand how a set of many different sensors, each with the same monolayer chemistry but different particle configurations, can act as arrays with more information content than expected. Differences in the swelling efficiencies of different volatile targets combine with different sensitivities of the networks to create patterns for chemical identification.

We conclude that the origins of configurational diversity are related to variations of particle connectivity in networks due to the particular arrangements of the constituent nanoparticles. We propose that swelling efficiency may depend on the local environments around particles leading to differences between sensor elements. Heterogeneity of the networks combine with properties of the analytes to produce new information that is difficult to measure directly, but is captured by machine learning algorithms.

Our Model 4 suggests that experiments to correlate particle arrangements with measured sensitivity could be useful to confirm the hypothesis, but such experiments would be very difficult since nanoparticle networks are difficult to image even with state-of-the-art microscopy. Moreover, even spectacular images would not provide direct information on connectivity. We also note that our model of neighbor dependent swelling could be modified to consider variations in other parameters like local barrier heights. Also, we could have modeled swelling as more efficient (instead of less efficient) in close packed arrangements and achieved a similar outcome. Thus, our conclusion is that neighbor connectivity matters, but we cannot specify exactly what properties are most sensitive to the particle arrangements. The simplest explanation is a relationship between connectivity and swelling.

4. Summary & Conclusions

In this work, we have demonstrated that nanoparticle based sensors can detect and classify many types of odorants including pure chemicals, Tea aromas, and solids relevant to explosives detection. Large sensor arrays take advantage of multivariate statistical methods and machine learning algorithms to achieve classification accuracies of 95-100% for large sets of test chemicals. Array functionality is demonstrated to be robust over a time period of at least 90 days. Sensors operate over a range of concentrations with > 90% classification accuracy. We demonstrate that nanoparticle sensors provide fast and reversible sensing with 'on' times quicker than 100 msec. Experiments with multi-particle sensor chips support a hypothesis that more sensing chemistries will allow larger test sets and further improvements of classification accuracy.

We have initiated a new modeling effort to harness the predictive capabilities of UNIFAC to provide rational design for new sensor materials. Initial data provide validation for the modeling approach with a qualitative match between experiment and theory. We discovered a new sensing mechanism based on structural diversity, which is associated with variability in how nanoparticles assemble onto electrodes to make working chemiresistors. Experimentally, we observe that sensor elements with identical materials and electrode structures can assemble into aggregates of different sizes, shapes, and particle arrangements. The different particle arrangements effectively act as different materials, adding non-redundant information to the pattern recognition capabilities of the overall array. A network model suggests that variations in swelling efficiency for different particle coordination contributes to configuration-induced sensor diversity.

Sensor fabrication is shown to be robust and reproducible, and sensing capabilities are broad, ranging from pure chemicals to complex aromas. Extrapolation of the current results suggests that our models can be used to design and optimize sensor materials for any targets of interest, including explosives, chemical precursors, and interferents. Expanding the number of sensor elements and sensor materials in combination with machine learning and fast calibration should provide highly effective chemical sensors for explosives detection and classification.